Shot Noise in Graphene

L. DiCarlo,[1] J. R. Williams,[2] Yiming Zhang,[1] D. T. McClure,[1] and C. M. Marcus[1]
[1]*Department of Physics, Harvard University, Cambridge, Massachusetts 02138, USA*
[2]*School of Engineering and Applied Sciences, Harvard University, Cambridge, Massachusetts 02138, USA*
(Received 20 November 2007; published 14 April 2008)

We report measurements of current noise in single-layer and multilayer graphene devices. In four single-layer devices, including a *p*-*n* junction, the Fano factor remains constant to within ±10% upon varying carrier type and density, and averages between 0.35 and 0.38. The Fano factor in a multilayer device is found to decrease from a maximal value of 0.33 at the charge-neutrality point to 0.25 at high carrier density. These results are compared to theories for shot noise in ballistic and disordered graphene.

DOI: 10.1103/PhysRevLett.100.156801 PACS numbers: 73.61.Wp, 73.50.Td

Shot noise, the temporal fluctuation of electric current out of equilibrium, originates from the partial transmission of quantized charge [1]. Mechanisms that can lead to shot noise in mesoscopic conductors include tunneling, quantum interference, and scattering from impurities and lattice defects. Shot noise yields information about transmission that is not available from the dc current alone.

In graphene [2,3], a zero-gap two-dimensional semimetal in which carrier type and density can be controlled by gate voltages [4], density-dependent shot-noise signatures under various conditions have been investigated theoretically [5,6]. For wide samples of ballistic graphene (width-to-length ratio $W/L \gtrsim 4$) the Fano factor, $\mathcal{F}$, i.e., the current noise normalized to the noise of Poissonian transmission statistics, is predicted to be $1/3$ at the charge-neutrality point and $\sim$0.12 in both electron (n) and hole (p) regimes [5]. The value $\mathcal{F} = 1 - 1/\sqrt{2} \approx 0.29$ is predicted for shot noise across a ballistic p-n junction [6]. For strong, smooth "charge-puddle" disorder, theory predicts $\mathcal{F} \approx 0.30$ both at and away from the charge-neutrality point, for all $W/L \gtrsim 1$ [7]. Disorder may thus have a similar effect on noise in graphene as in diffusive metals, where $\mathcal{F}$ is universally $1/3$ [8–13] regardless of shape and carrier density. Recent theory investigates numerically the evolution from a density-dependent to a density-independent $\mathcal{F}$ with increasing disorder [14]. To our knowledge, experimental data for shot noise in graphene has not yet been reported.

This Letter presents an experimental study of shot noise in graphene at low temperatures and zero magnetic field. Data for five devices, including a locally-gated p-n junction, are presented. For three globally-gated, single-layer samples, we find $\mathcal{F} \sim 0.35$–0.37 in both electron and hole doping regions, with essentially no dependence on electronic sheet density, n_s, in the range $|n_s| \lesssim 10^{12}$ cm^{-2}. Similar values are obtained for a locally-gated single-layer p-n junction in both unipolar (n-n or p-p) and bipolar (p-n or n-p) regimes. In a multilayer sample, the observed $\mathcal{F}$ evolves from 0.33 at the charge-neutrality point to 0.25 at $n_s \sim 6 \times 10^{12}$ cm^{-2}.

Devices were fabricated by mechanical exfoliation of highly-oriented pyrolytic graphite [4]. Exfoliated sheets were deposited on a degenerately-doped Si substrate capped with 300 nm of thermally grown SiO_2. Regions identified by optical microscopy as potential single-layer graphene were contacted with thermally evaporated Ti/Au leads (5/40 nm) patterned by electron-beam lithography. Additional steps in the fabrication of the p-n junction device are detailed in Ref. [15]. Devices were measured in two ^{3}He cryostats, one allowing dc (lock-in) transport measurements in fields $|B_\perp| \leq 8$ T perpendicular to the graphene plane, and another allowing simultaneous measurements of dc transport and noise [16] near 1.5 MHz, but limited to $B_\perp \sim 0$.

Differential resistance $R = dV_{sd}/dI$ (I is the current and V_{sd} is the source-drain voltage) of a wide, short sample [A1, $(W, L) = (2.0, 0.35)$ μm] is shown as a function of back-gate voltage V_{bg} at $V_{sd} = 0$ and $B_\perp = 0$ in Fig. 1(a). While the width of the peak is consistent with A1 being single-layer graphene [17,18], more direct evidence is obtained from the quantum Hall (QH) signature shown in Fig. 1(b). The image shows differential conductance $g = 1/R$ as a function of V_{bg} and $B_\perp$, following subtraction of the best-fit quadratic polynomial to $g(V_{bg})$ at each $B_\perp$ setting to maximize contrast. Dashed lines correspond to filling factors $n_s h/eB_\perp = 6$, 10, 14, and 18, with $n_s = \alpha(V_{bg} + 1.1\text{ V})$ and lever arm $\alpha = 6.7 \times 10^{10}$ cm^{-2}/V. Their alignment with local minima in $\delta g(V_{bg})$ identifies A1 as single-layer graphene [19,20]. The Drude mean free path $\ell = h/2e^2 \cdot \sigma/k_F$ [21], where $k_F = \sqrt{\pi|n_s|}$, is found to be $\sim$40 nm away from the charge-neutrality point using the $B_\perp = 0$ conductivity $\sigma = (RW/L)^{-1}$ [Fig. 2(a) inset].

Current noise spectral density S_I is measured using a cross-correlation technique described in Ref. [16] [see Fig. 1(c)]. Following calibration of amplifier gains and electron temperature T_e using Johnson noise thermometry (JNT) for each cooldown, the excess noise $S_I^e \equiv S_I - 4k_B T_e g(V_{sd})$ is extracted. $S_I^e(V_{sd})$ for sample A1 is shown in Fig. 2(a). Linearity of S_I^e at high bias indicates negligible extrinsic ($1/f$ or telegraph) resistance fluctuations within the measurement bandwidth. For these data, a

 © 2008 The American Physical Society

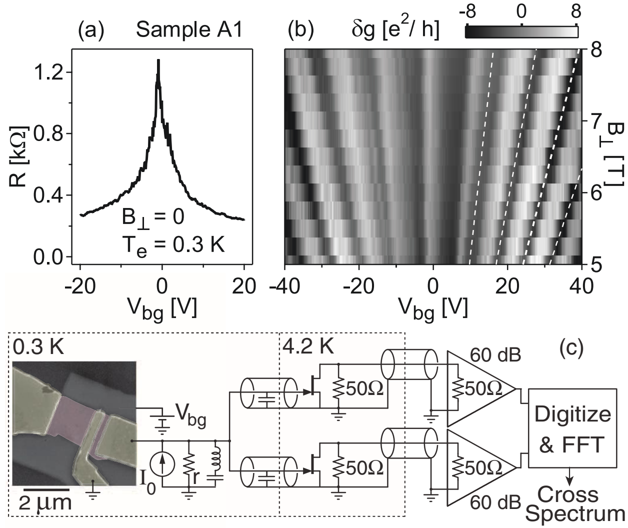

FIG. 1 (color online). (a) Differential resistance R of sample A1 as a function of back-gate voltage V_{bg} at electron temperature $T_e = 0.3$ K, perpendicular field $B_\perp = 0$, and source-drain voltage $V_{\mathrm{sd}} = 0$. (b) Differential two-terminal conductance $g(V_{\mathrm{sd}} = 0)$ as a function of $B_\perp$ and V_{bg} in the QH regime, after subtracting a quadratic fit at each $B_\perp$. Lines of constant filling factors 6, 10, 14, and 18 (dashed lines) indicate a single-layer sample. (c) Equivalent circuit near 1.5 MHz of the system measuring current noise using cross correlation of two channels [16]. Current bias I_o contains a 7.5 $\mathrm{nA_{rms}}$, 20 Hz part for lock-in measurements and a controllable dc part generating the dc component of V_{sd} via the shunt resistance $r = 5$ kΩ. Scanning electron micrograph of a three-lead pattern defining two devices similar to A1 and A2.

single-parameter fit to the scattering-theory form (for energy-independent transmission) [22,23],

$$S_I^e = 2eI\mathcal{F}\left[\coth\left(\frac{eV_{\mathrm{sd}}}{2k_BT_e}\right) - \frac{2k_BT_e}{eV_{\mathrm{sd}}}\right], \qquad (1)$$

gives a best-fit Fano factor $\mathcal{F} = 0.349$. Simultaneously measured conductance $g \approx 22.2e^2/h$ was independent of bias within $\pm 0.5\%$ (not shown) in the $|V_{\mathrm{sd}}| \leq 350$ μV range used for the fit. Note that the observed quadratic-to-linear crossover agrees well with that in the curve fit, indicating weak inelastic scattering in A1 [11,12], and negligible series resistance (e.g., from contacts), which would broaden the crossover by reducing the effective V_{sd} across the sample.

Figure 2(b) shows similarly measured values for $\mathcal{F}$ as a function of V_{bg}. $\mathcal{F}$ is observed to remain nearly constant for $|n_s| \lesssim 10^{12}$ cm^{-2}. Over this density range, the average $\mathcal{F}$ is 0.35 with standard deviation 0.01. The estimated error in the best-fit $\mathcal{F}$ at each V_{bg} setting is ± 0.002, comparable to the marker size and smaller than the variation in $\mathcal{F}$ near $V_{\mathrm{bg}} = 0$, which we believe results from mesoscopic fluctuations of $\mathcal{F}$. Nearly identical noise results (not shown) were found for a similar sample (B), with dimensions

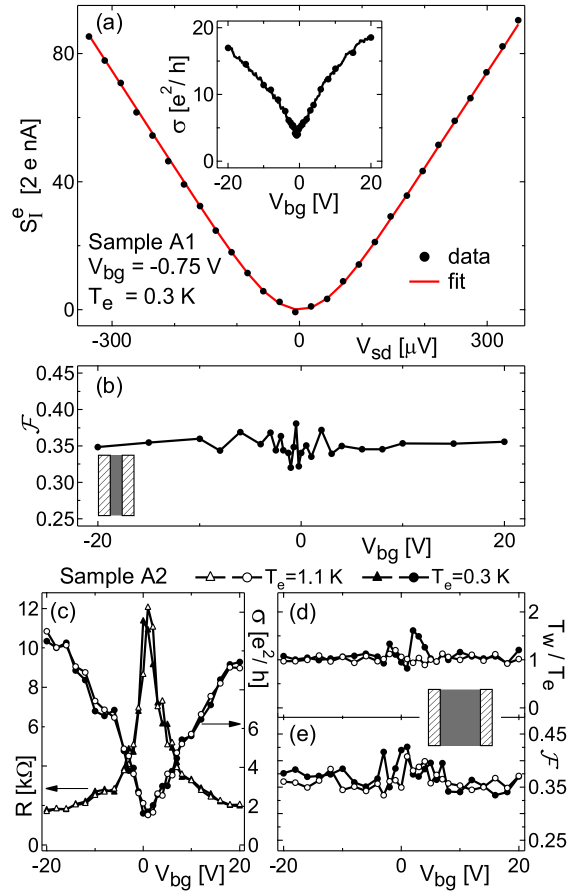

FIG. 2 (color online). (a) Inset: Conductivity $\sigma = (RW/L)^{-1}$ calculated using $R(V_{\mathrm{bg}})$ data in Fig. 1(a) and $W/L = 5.7$. Solid circles correspond to $\sigma(V_{\mathrm{sd}} = 0)$ at the V_{bg} settings of noise measurements shown in (b). Main: Excess noise S_I^e as function of V_{sd} near the charge-neutrality point, $V_{\mathrm{bg}} = -0.75$ V. The solid curve is the single-parameter best fit to Eq. (1), giving Fano factor $\mathcal{F} = 0.349$ (using $T_e = 303$ mK as calibrated by JNT). (b) Best-fit $\mathcal{F}$ at 25 V_{bg} settings across the charge-neutrality point for electron and hole densities reaching $|n_s| \sim 1.4 \times 10^{12}$ cm^{-2}. (c) R (left axis) and σ (right axis) of sample A2 as a function of V_{bg} ($W/L = 1.4$), with $V_{\mathrm{sd}} = 0$, at 0.3 K (solid markers) and at 1.1 K (open markers). (d),(e) Crossover width T_w (normalized to JNT-calibrated T_e) and $\mathcal{F}$, obtained from best fits using Eq. (1) to $S_I^e(V_{\mathrm{sd}})$ data over $|V_{\mathrm{sd}}| \leq 350(650)$ μV for $T_e = 0.3(1.1)$ K.

(2.0, 0.3) μm and a QH signature consistent with a single layer.

Transport and noise data for a more square single-layer sample [A2, patterned on the same graphene sheet as A1, with dimensions (1.8, 1.3) μm] at $T_e = 0.3$ K (solid circles) and $T_e = 1.1$ K (open circles) are shown in Figs. 2(c)–2(e). At both temperatures, the conductivity shows $\sigma_{\min} \approx 1.5e^2/h$ and gives $\ell \sim 25$ nm away from the charge-neutrality point. That these two values differ from those in sample A1 is particularly notable as samples A1 and A2 were patterned on the same piece of graphene. Results of fitting Eq. (1) to $S_I^e(V_{\mathrm{sd}})$ for sample A2 are

shown in Figs. 2(d) and 2(e). To allow for possible broadening of the quadratic-to-linear crossover by series resistance and/or inelastic scattering, we treat electron temperature as a second fit parameter (along with $\mathcal{F}$) and compare the best-fit value, T_w, with the T_e obtained from Johnson noise. Figure 2(d) shows T_w tracking the calibrated T_e at both temperatures. Small deviation of T_w/T_e from unity near the charge-neutrality point at $T_e = 0.3$ K can be attributed to conductance variations up to $\pm 20\%$ in the fit range $|V_{\rm sd}| \leq 350$ μV at these values of $V_{\rm bg}$. As in sample A1, $\mathcal{F}$ is found to be independent of carrier type and density over $|n_s| \lesssim 10^{12}$ cm^{-2}, averaging 0.37(0.36) with standard deviation 0.02(0.02) at $T_e = 0.3(1.1)$ K. Evidently, despite its different aspect ratio, A2 exhibits a noise signature similar to that of A1.

The lack of R-dependence in $\mathcal{F}$ suggests that bias-dependent electron heating in the metallic reservoirs [12] is negligible for our samples. This type of heating, originating from imperfect dissipation of the generated power $V_{\rm sd}^2/R$, can affect shot noise measurements since these require $|V_{\rm sd}|$ several times the thermal voltage (here, $e|V_{\rm sd}|/k_B T_e \lesssim 10$). In the presence of heating, fitting the excess noise $S_I[V_{\rm sd}, T_e + \Delta T_e(V_{\rm sd})] - 4k_B T_e g$ to Eq. (1) would overestimate $\mathcal{F}$. The nearly equal values of $\mathcal{F}$ observed in A1 and A2 despite the factor $\sim$10 difference in R at comparable n_s suggest that heating in the reservoirs is negligible [24].

Transport and noise measurements for a single-layer graphene p-n junction [15], sample C, are shown in Fig. 3. The image in Fig. 3(a) shows differential resistance R as a function of $V_{\rm bg}$ and local top-gate voltage $V_{\rm tg}$. The two gates allow independent control of charge densities in adjacent regions of the device [see Fig. 3(c) inset]. In the bipolar regime, the best-fit $\mathcal{F}$ shows little density dependence and averages 0.38, equal to the average value deep in the unipolar regime, and similar to results for the back-gate-only single-layer samples (A1, A2, and B). Close to charge neutrality in either region (though particularly in the region under the top gate), $S_I^e(V_{\rm sd})$ deviates from the form of Eq. (1) (data not shown). This is presumably due to resistance fluctuation near charge neutrality, probably due mostly to mobile traps in the Al_2O_3 insulator beneath the top gate.

Measurements at 0.3 K and at 1.1 K for sample D, of dimensions (1.8, 1.0) μm, are shown in Fig. 4. A $\sim$3 nm step height between SiO_2 and carbon surfaces measured by atomic force microscopy prior to electron-beam lithography [25] suggests this device is likely multilayer. Further indications include the broad $R(V_{\rm bg})$ peak [26] and the large minimum conductivity, $\sigma_{\rm min} \sim 8e^2/h$ at $B_\perp = 0$ [Fig. 4(a)], as well as the absence of QH signature for $|B_\perp| \leq 8$ T at 250 mK (not shown). Two-parameter fits of $S_I^e(V_{\rm sd})$ data to Eq. (1) show three notable differences from results in the single-layer samples [Figs. 4(b) and 4(c)]: First, $\mathcal{F}$ shows a measurable dependence on back-gate voltage, decreasing from 0.33 at the charge-neutrality point

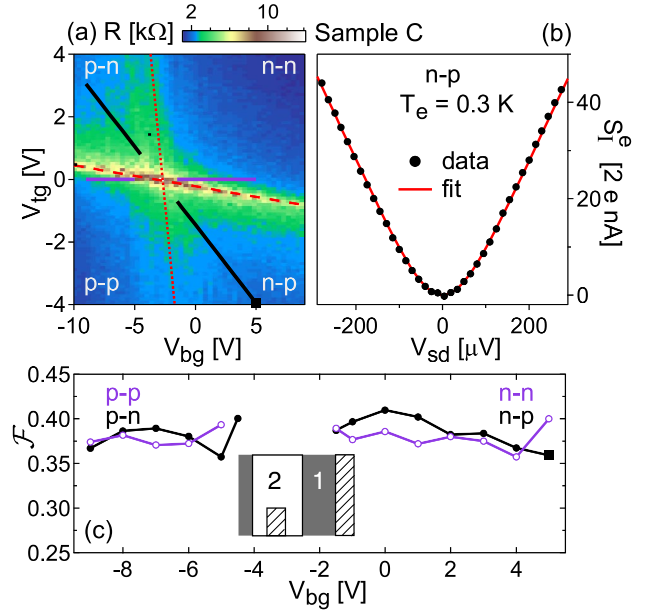

FIG. 3 (color online). (a) Differential resistance R of sample C, a single-layer p-n junction, as a function of back-gate voltage $V_{\rm bg}$ and top-gate voltage $V_{\rm tg}$. The skewed-cross pattern defines quadrants of n and p carriers in regions 1 and 2. Dotted and dashed lines indicate charge neutrality in regions 1 and 2, respectively. (b) $S_I^e(V_{\rm sd})$ measured in n-p regime with $(V_{\rm bg}, V_{\rm tg}) = (5, -4)$ V (solid dots) and best fit to Eq. (1) (curve), with $\mathcal{F} = 0.36$. (c) Main: Best-fit $\mathcal{F}$ along the cuts shown in (a), at which $n_{s1} \sim n_{s2}$ (open symbols) and $n_{s1} \sim -4n_{s2}$ (solid symbols). Inset: Schematic of the device. The top gate covers region 2 and one of the contacts.

to 0.25 at $n_s \sim 6 \times 10^{12}$ cm^{-2} for $T_e = 0.3$ K; second, $\mathcal{F}$ decreases with increasing temperature; finally, T_w/T_e is 1.3–1.6 instead of very close to 1. We interpret the last two differences, as well as the sublinear dependence of S_I^e on $V_{\rm sd}$ (see Fig. 4 inset), as indicating sizable inelastic scattering [8,9] in sample D. (An alternative explanation in terms of series resistance would require it to be density, bias, and temperature dependent, which is inconsistent with the independence of g on $V_{\rm sd}$ and T_e).

Summarizing the experimental results, we find that in four single-layer samples, $\mathcal{F}$ is insensitive to carrier type and density, temperature, aspect ratio, and the presence of a p-n junction. In one multilayer sample, $\mathcal{F}$ does depend on density and temperature, and $S_I^e(V_{\rm sd})$ shows a broadened quadratic-to-linear crossover and is sublinear in $V_{\rm sd}$ at high bias. We may now compare these results to expectations based on theoretical and numerical results for ballistic and disordered graphene.

Theory for ballistic single-layer graphene with $W/L \gtrsim 4$ gives a universal $\mathcal{F} = 1/3$ at the charge-neutrality point, where transmission is evanescent, and $\mathcal{F} \sim 0.12$ for $|n_s| \gtrsim \pi/L^2$, where propagating modes dominate transmission [5]. While the measured $\mathcal{F}$ at the charge-neutrality point in samples A1 and B ($W/L = 5.7$ and 6.7, respectively) is consistent with this prediction, the absence of density

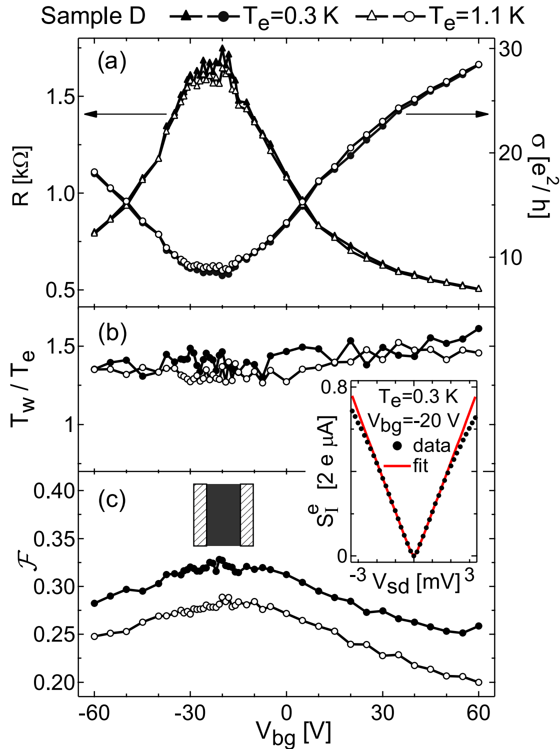

FIG. 4 (color online). (a) Differential resistance R (left axis) and conductivity σ (right axis) of sample D as a function of $V_{\rm bg}$, with $V_{\rm sd} = 0$, at 0.3 K (solid markers) and at 1.1 K (open markers). (b),(c) Best-fit T_w (normalized to JNT-calibrated T_e) and $\mathcal{F}$ to $S_I^e(V_{\rm sd})$ data over $|V_{\rm sd}| \leq 0.5(1)$ mV for $T_e = 0.3(1.1)$ K. Inset: Sublinear dependence of S_I^e on $V_{\rm sd}$ is evident in data taken over a larger bias range. Solid curve is the two-parameter best fit of Eq. (1) over $|V_{\rm sd}| \leq 0.5$ mV.

dependence is not: $\pi/L^2 \sim 3 \times 10^9$ cm^{-2} is well within the range of carrier densities covered in the measurements. Theory [27] for ballistic graphene contacted with finite-density leads finds slight increments of $\mathcal{F}$ from 1/3 at the charge-neutrality point, in agreement with this experiment. However, $\mathcal{F}$ in this contact model remains density dependent. Theory for ballistic graphene p-n junctions [6] predicts $\mathcal{F} \approx 0.29$, lower than the value $\sim$0.38 observed in sample C in both p-n and n-p regimes. We speculate that these discrepancies likely arise from the presence of disorder. Numerical results for strong, smooth disorder [7] predict a constant $\mathcal{F}$ at and away from the charge-neutrality point for $W/L \gtrsim 1$, consistent with experiment. However, the predicted value $\mathcal{F} \approx 0.30$ is $\sim$20% lower than observed in all single-layer devices. Recent numerical simulations [14] of small samples ($L = W \sim 10$ nm) investigate the vanishing of carrier dependence in $\mathcal{F}$ with increasing disorder strength. In the regime where disorder makes $\mathcal{F}$ density independent, the value $\mathcal{F} \sim 0.35$–0.40 is found to depend weakly on disorder strength and sample size.

Since theory for an arbitrary number of layers is not available for comparison to noise results in the multilayer sample D, we compare only to existing theory for ballistic bilayer graphene [28]. It predicts $\mathcal{F} = 1/3$ over a much narrower density range than for the single layer, and abrupt features in $\mathcal{F}$ at finite density due to transmission resonances. A noise theory beyond the bilayer ballistic regime may thus be necessary to explain the observed smooth decrease of $\mathcal{F}$ with increasing density in sample D.

We thank C. H. Lewenkopf, L. S. Levitov, and D. A. Abanin for useful discussions. This research was supported in part by IBM (L. D. C.), INDEX, an NRI Center, and Harvard NSEC.

[1] Y. M. Blanter and M. Büttiker, Phys. Rep. **336**, 1 (2000).
[2] A. K. Geim and K. S. Novoselov, Nat. Mater. **6**, 183 (2007).
[3] A. H. Castro Neto *et al.*, arXiv:0709.1163 [Rev. Mod. Phys. (to be published)].
[4] K. S. Novoselov *et al.*, Science **306**, 666 (2004).
[5] J. Tworzydło *et al.*, Phys. Rev. Lett. **96**, 246802 (2006).
[6] V. V. Cheianov and V. I. Fal'ko, Phys. Rev. B **74**, 041403(R) (2006).
[7] P. San-Jose, E. Prada, and D. S. Golubev, Phys. Rev. B **76**, 195445 (2007).
[8] C. W. J. Beenakker and M. Büttiker, Phys. Rev. B **46**, 1889(R) (1992).
[9] M. J. M. de Jong and C. W. J. Beenakker, Phys. Rev. B **46**, 13400 (1992).
[10] Y. V. Nazarov, Phys. Rev. Lett. **73**, 134 (1994).
[11] A. H. Steinbach, J. M. Martinis, and M. H. Devoret, Phys. Rev. Lett. **76**, 3806 (1996).
[12] M. Henny *et al.*, Phys. Rev. B **59**, 2871 (1999).
[13] R. J. Schoelkopf *et al.*, Phys. Rev. Lett. **78**, 3370 (1997).
[14] C. H. Lewenkopf, E. R. Mucciolo, and A. H. Castro Neto, Phys. Rev. B **77**, 081410(R) (2008).
[15] J. R. Williams, L. DiCarlo, and C. M. Marcus, Science **317**, 638 (2007).
[16] L. DiCarlo *et al.*, Rev. Sci. Instrum. **77**, 073906 (2006).
[17] K. S. Novoselov *et al.*, Nature (London) **438**, 197 (2005).
[18] Y. Zhang *et al.*, Nature (London) **438**, 201 (2005).
[19] E. McCann and V. I. Fal'ko, Phys. Rev. Lett. **96**, 086805 (2006).
[20] J. Martin *et al.*, Nature Phys. **4**, 144 (2008).
[21] A. Rycerz, J. Tworzydło, and C. W. J. Beenakker, Europhys. Lett. **79**, 57003 (2007).
[22] G. B. Lesovik, Pis'ma Zh. Eksp. Teor. Fiz. **49**, 513 (1989) [JETP Lett. **49**, 592 (1989)].
[23] M. Büttiker, Phys. Rev. B **46**, 12485 (1992).
[24] Effects of reservoir heating on noise have been observed in diffusive wires ($R \sim 10\ \Omega$) with metallic contacts [12]. The generated power in our graphene samples is weaker by 1–3 orders of magnitude, which could explain why heating of the metallic contacts appears negligible in this experiment.
[25] D. Graf *et al.*, Phys. Rev. B **75**, 245429 (2007).
[26] Y. Zhang *et al.*, Phys. Rev. Lett. **94**, 176803 (2005).
[27] H. Schomerus, Phys. Rev. B **76**, 045433 (2007).
[28] I. Snyman and C. W. J. Beenakker, Phys. Rev. B **75**, 045322 (2007).